Title

Extraction of the U235 and Pu239 Antineutrino Spectra at Daya Bay

Permalink

Journal

ISSN

Authors

Adey, D
An, FP
Balantekin, AB
et al.

Publication Date

DOI

Copyright Information

Peer reviewed

Measurement of Individual Antineutrino Spectra from ^{235}U and ^{239}Pu at Daya Bay

D. Adey,[1] F. P. An,[2] A. B. Balantekin,[3] H. R. Band,[4] M. Bishai,[5] S. Blyth,[6] D. Cao,[7] G. F. Cao,[1] J. Cao,[1] J. F. Chang,[1] Y. Chang,[8] H. S. Chen,[1] S. M. Chen,[9] Y. Chen,[10, 11] Y. X. Chen,[12] J. Cheng,[1] Z. K. Cheng,[11] J. J. Cherwinka,[3] M. C. Chu,[13] A. Chukanov,[14] J. P. Cummings,[15] N. Dash,[1] F. S. Deng,[16] Y. Y. Ding,[1] M. V. Diwan,[5] T. Dohnal,[17] J. Dove,[18] M. Dvořák,[17] D. A. Dwyer,[19] M. Gonchar,[14] G. H. Gong,[9] H. Gong,[9] W. Q. Gu,[5] J. Y. Guo,[11] L. Guo,[9] X. H. Guo,[20] Y. H. Guo,[21] Z. Guo,[9] R. W. Hackenburg,[5] S. Hans,[5, *] M. He,[1] K. M. Heeger,[4] Y. K. Heng,[1] A. Higuera,[22] Y. K. Hor,[11] Y. B. Hsiung,[6] B. Z. Hu,[6] J. R. Hu,[1] T. Hu,[1] Z. J. Hu,[11] H. X. Huang,[23] X. T. Huang,[24] Y. B. Huang,[1] P. Huber,[25] D. E. Jaffe,[5] K. L. Jen,[26] X. L. Ji,[1] X. P. Ji,[5] R. A. Johnson,[27] D. Jones,[28] L. Kang,[29] S. H. Kettell,[5] L. W. Koerner,[22] S. Kohn,[30] M. Kramer,[19, 30] T. J. Langford,[4] J. Lee,[19] J. H. C. Lee,[31] R. T. Lei,[29] R. Leitner,[17] J. K. C. Leung,[31] C. Li,[24] F. Li,[1] H. L. Li,[1] Q. J. Li,[1] S. Li,[29] S. C. Li,[25] S. J. Li,[11] W. D. Li,[1] X. N. Li,[1] X. Q. Li,[32] Y. F. Li,[1] Z. B. Li,[11] H. Liang,[16] C. J. Lin,[19] G. L. Lin,[26] S. Lin,[29] J. J. Ling,[11] J. M. Link,[25] L. Littenberg,[5] B. R. Littlejohn,[33] J. C. Liu,[1] J. L. Liu,[34] Y. Liu,[24] Y. H. Liu,[7] C. Lu,[35] H. Q. Lu,[1] J. S. Lu,[1] K. B. Luk,[30, 19] X. B. Ma,[12] X. Y. Ma,[1] Y. Q. Ma,[1] C. Marshall,[19] D. A. Martinez Caicedo,[33] K. T. McDonald,[35] R. D. McKeown,[36, 37] I. Mitchell,[22] L. Mora Lepin,[38] J. Napolitano,[28] D. Naumov,[14] E. Naumova,[14] J. P. Ochoa-Ricoux,[38, 39] A. Olshevskiy,[14] H.-R. Pan,[6] J. Park,[25] S. Patton,[19] V. Pec,[17] J. C. Peng,[18] L. Pinsky,[22] C. S. J. Pun,[31] F. Z. Qi,[1] M. Qi,[7] X. Qian,[5] N. Raper,[11] J. Ren,[23] R. Rosero,[5] B. Roskovec,[39] X. C. Ruan,[23] H. Steiner,[30, 19] J. L. Sun,[40] K. Treskov,[14] W.-H. Tse,[13] C. E. Tull,[19] B. Viren,[5] V. Vorobel,[17] C. H. Wang,[8] J. Wang,[11] M. Wang,[24] N. Y. Wang,[20] R. G. Wang,[1] W. Wang,[11, 37] W. Wang,[7] X. Wang,[41] Y. Wang,[7] Y. F. Wang,[1] Z. Wang,[1] Z. Wang,[9] Z. M. Wang,[1] H. Y. Wei,[5] L. H. Wei,[1] L. J. Wen,[1] K. Whisnant,[42] C. G. White,[33] H. L. H. Wong,[30, 19] S. C. F. Wong,[11] E. Worcester,[5] Q. Wu,[24] W. J. Wu,[1] D. M. Xia,[43] Z. Z. Xing,[1] J. L. Xu,[1] T. Xue,[9] C. G. Yang,[1] L. Yang,[29] M. S. Yang,[1] Y. Z. Yang,[9] M. Ye,[1] M. Yeh,[5] B. L. Young,[42] H. Z. Yu,[11] Z. Y. Yu,[1] B. B. Yue,[11] S. Zeng,[1] Y. Zeng,[11] L. Zhan,[1] C. Zhang,[5] C. C. Zhang,[1] F. Y. Zhang,[34] H. H. Zhang,[11] J. W. Zhang,[1] Q. M. Zhang,[21] R. Zhang,[7] X. F. Zhang,[1] X. T. Zhang,[1] Y. M. Zhang,[11] Y. M. Zhang,[9] Y. X. Zhang,[40] Y. Y. Zhang,[34] Z. J. Zhang,[29] Z. P. Zhang,[16] Z. Y. Zhang,[1] J. Zhao,[1] L. Zhou,[1] H. L. Zhuang,[1] and J. H. Zou[1]

(The Daya Bay Collaboration)

[1]*Institute of High Energy Physics, Beijing*
[2]*Institute of Modern Physics, East China University of Science and Technology, Shanghai*
[3]*University of Wisconsin, Madison, Wisconsin 53706*
[4]*Wright Laboratory and Department of Physics, Yale University, New Haven, Connecticut 06520*
[5]*Brookhaven National Laboratory, Upton, New York 11973*
[6]*Department of Physics, National Taiwan University, Taipei*
[7]*Nanjing University, Nanjing*
[8]*National United University, Miao-Li*
[9]*Department of Engineering Physics, Tsinghua University, Beijing*
[10]*Shenzhen University, Shenzhen*
[11]*Sun Yat-Sen (Zhongshan) University, Guangzhou*
[12]*North China Electric Power University, Beijing*
[13]*Chinese University of Hong Kong, Hong Kong*
[14]*Joint Institute for Nuclear Research, Dubna, Moscow Region*
[15]*Siena College, Loudonville, New York 12211*
[16]*University of Science and Technology of China, Hefei*
[17]*Charles University, Faculty of Mathematics and Physics, Prague*
[18]*Department of Physics, University of Illinois at Urbana-Champaign, Urbana, Illinois 61801*
[19]*Lawrence Berkeley National Laboratory, Berkeley, California 94720*
[20]*Beijing Normal University, Beijing*
[21]*Department of Nuclear Science and Technology, School of Energy and Power Engineering, Xi'an Jiaotong University, Xi'an*
[22]*Department of Physics, University of Houston, Houston, Texas 77204*
[23]*China Institute of Atomic Energy, Beijing*
[24]*Shandong University, Jinan*
[25]*Center for Neutrino Physics, Virginia Tech, Blacksburg, Virginia 24061*
[26]*Institute of Physics, National Chiao-Tung University, Hsinchu*
[27]*Department of Physics, University of Cincinnati, Cincinnati, Ohio 45221*
[28]*Department of Physics, College of Science and Technology, Temple University, Philadelphia, Pennsylvania 19122*
[29]*Dongguan University of Technology, Dongguan*
[30]*Department of Physics, University of California, Berkeley, California 94720*
[31]*Department of Physics, The University of Hong Kong, Pokfulam, Hong Kong*
[32]*School of Physics, Nankai University, Tianjin*
[33]*Department of Physics, Illinois Institute of Technology, Chicago, Illinois 60616*
[34]*Department of Physics and Astronomy, Shanghai Jiao Tong University, Shanghai Laboratory for Particle Physics and Cosmology, Shanghai*

[35]*Joseph Henry Laboratories, Princeton University, Princeton, New Jersey 08544*
[36]*California Institute of Technology, Pasadena, California 91125*
[37]*College of William and Mary, Williamsburg, Virginia 23187*
[38]*Instituto de Física, Pontificia Universidad Católica de Chile, Santiago*
[39]*Department of Physics and Astronomy, University of California, Irvine, California 92697*
[40]*China General Nuclear Power Group, Shenzhen*
[41]*College of Electronic Science and Engineering, National University of Defense Technology, Changsha*
[42]*Iowa State University, Ames, Iowa 50011*
[43]*Chongqing University, Chongqing*
(Dated: April 17, 2019)

This letter reports a new measurement of the prompt energy spectrum of reactor antineutrinos and the first measurement of individual spectra from ^{235}U and ^{239}Pu at Daya Bay. The analysis uses 3.5 million inverse beta decay (IBD) candidates in four near antineutrino detectors in 1958 days. The shape of the measured IBD prompt energy spectrum disagrees with the prediction of the Huber-Mueller model at 5.3σ. In the energy range of 4–6 MeV, a maximal local discrepancy of 6.3σ is observed. The individual spectra of the two dominant isotopes, ^{235}U and ^{239}Pu, are extracted using the evolution of the prompt spectrum as a function of the isotope fission fractions. In the energy window of 4–6 MeV, a 7% (9%) excess of events is observed for the ^{235}U (^{239}Pu) spectrum compared with the normalized Huber-Mueller model prediction.

Nuclear reactors are powerful sources of electron antineutrinos ($\bar{\nu}_e$) and have played an important role in neutrino physics. Most recently, Daya Bay [1–6], RENO [7, 8], and Double Chooz [9, 10] reported observations of neutrino oscillation induced by a non-zero mixing angle θ_{13}. In addition, these experiments also provided measurements of reactor $\bar{\nu}_e$ flux and spectrum [11–14] at distances of 300–500 m from the reactors. The flux measurements confirmed the ∼6% deficit found in the 2011 re-evaluation [15, 16] of the reactor $\bar{\nu}_e$ flux ("Reactor Antineutrino Anomaly" [17]). The measurement of an evolution of reactor $\bar{\nu}_e$ flux with the fission fractions at Daya Bay suggested that ^{235}U, among the four major isotopes (^{235}U, ^{239}Pu, ^{238}U and ^{241}Pu), may be the primary contributor to the flux anomaly [18]. The spectral measurements indicated a new anomaly ("5-MeV bump") when compared with theoretical calculations, an observation further confirmed by NEOS [19], and by re-examination of earlier reactor antineutrino data [20]. Observation of evolution of the reactor $\bar{\nu}_e$ spectrum from commercial reactors [18, 21–23] and measurement of the ^{235}U $\bar{\nu}_e$ spectrum from highly enriched uranium research reactors [24, 25] have also been performed, providing first glimpses at the dependence of spectral features on reactor fuel content. Additional precision measurements are essential to fully investigate the origins of the reactor $\bar{\nu}_e$ flux and spectrum anomalies, and provide crucial inputs to future reactor neutrino experiments [26].

This letter reports a new measurement of the prompt energy spectrum of reactor $\bar{\nu}_e$ at Daya Bay with three times more $\bar{\nu}_e$ events and reduced systematic uncertainties compared with previous results [12]. Furthermore, the individual prompt energy spectra of two dominant isotopes (^{235}U and ^{239}Pu) are obtained for the first time by fitting the evolution of the prompt energy spectrum as a function of fission fractions from commercial reactors. A combined measurement of the ^{239}Pu and ^{241}Pu spectra is also reported with uncertainties reduced from that obtained for ^{239}Pu alone.

The Daya Bay Reactor Neutrino Experiment is located near the Daya Bay nuclear power complex, which hosts six commercial pressurized-water reactors (2.9 GW maximum thermal power). Identically designed $\bar{\nu}_e$ detectors (ADs) are deployed in two near halls (EH1 and EH2) containing two ADs each and in the far hall (EH3) with four ADs. Each AD contains 20 tons of gadolinium-doped liquid scintillator (GdLS) serving as the primary $\bar{\nu}_e$ target. The analysis uses 1958 days of data from four near ADs which involves four to six refueling cycles for each reactor core. Details about the experiment and the data set are given in Ref. [6, 27].

In a typical commercial reactor, antineutrinos are produced from thousands of beta decay branches of the fission products. The $\bar{\nu}_e$ spectrum is measured with inverse beta decay (IBD) reactions: $\bar{\nu}_e + p \rightarrow e^+ + n$. The predicted $\bar{\nu}_e$ energy spectrum in a detector at a given time t is calculated as

$$S_d(E_\nu, t) = N_d \epsilon_d \sigma(E_\nu) \sum_r \frac{P_{ee}(E_\nu, L_{rd})}{4\pi L_{rd}^2} \frac{\mathrm{d}\phi_r(E_\nu, t)}{\mathrm{d}E_\nu \mathrm{d}t}, \quad (1)$$

where E_ν is the $\bar{\nu}_e$ energy, d is the detector index, r is the reactor index, N_d is the target proton number, ϵ_d is the detection efficiency, L_{rd} is the distance from detector d to reactor r, $P_{ee}(E_\nu, L_{rd})$ is the $\bar{\nu}_e$ survival probability in the standard three-neutrino model, and $\sigma(E_\nu)$ is the IBD cross section. The energy spectrum of antineutrinos from one reactor is

$$\begin{aligned}
\frac{\mathrm{d}\phi_r(E_\nu, t)}{\mathrm{d}E_\nu \mathrm{d}t} &= \frac{W_r(t)}{\sum_i f_{ir}(t)e_i} \sum_i f_{ir}(t)s_i(E_\nu)c_i^{ne}(E_\nu, t) \\
&\quad + s_{\mathrm{SNF}}(E_\nu, t) + s_{\mathrm{NL}}(E_\nu, t),
\end{aligned} \quad (2)$$

where $W_r(t)$ is the thermal power of reactor r, e_i is the energy released per fission for isotope i, $f_{ir}(t)$ is the fission fraction, $s_i(E_\nu)$ is the $\bar{\nu}_e$ energy spectrum per fission for each isotope, $c_i^{ne}(E_\nu, t)$ is a function of the order of unity absorbing the correction to the energy spectrum due to nonequilibrium effects of long-lived fission fragments, $s_{\mathrm{SNF}}(E_\nu, t)$ and $s_{\mathrm{NL}}(E_\nu, t)$ are contributions from spent nuclear fuel (SNF)

and from nuclides with $\bar{\nu}_e$ flux with a nonlinear dependence on reactor neutron flux [28], respectively.

For $s_i(E_\nu)$ in Eq. 2, the ^{235}U, ^{239}Pu, and ^{241}Pu $\bar{\nu}_e$ spectra from Huber [16] and ^{238}U spectrum from Mueller [15] are used in the prediction (Huber-Mueller model). Thermal power and fission fraction data are provided by the Daya Bay nuclear power plant with uncertainties of 0.5% and 5% [12], respectively. The correlations of fission fractions among the four isotope are taken from Ref. [12]. The energies released per fission (e_i) are taken from Ref. [29].

In contrast to previous Daya Bay analyses, the nonequilibrium correction and contributions from SNF and nonlinear nuclides are estimated and added to the flux prediction with time evolution. Long-lived fission fragments are accumulated during the fuel burning and are not in equilibrium for fresh fuel at the start of each refueling cycle. The nonequilibrium effect exists for ILL measurements [30–32], which are the basis of the Huber-Mueller model, due to a limited irradiation time. The correction of the nonequilibrium effect (0.7%) for each batch of fuel elements is calculated daily based on the irradiation time [15]. The SNF (0.2%), including contribution from the storage water pool and the shutdown reactor core, is calculated daily using the refueling history provided by the power plant. The $\bar{\nu}_e$ flux from some nuclides has a nonlinear dependence on the neutron flux in a reactor core [28]. The correction for these nonlinear nuclides is obtained as a function of time based on information provided by the power plant and contributes $<0.1\%$ of the total $\bar{\nu}_e$ flux.

The ~ 3.5 million IBD candidates in the four near ADs and the expected backgrounds from Ref. [6] are used in this analysis. The accidental and Am-C correlated backgrounds are estimated daily in each AD. The cosmogenic ^{9}Li/^{8}He, fast neutron, and ^{13}C(α, n)^{16}O backgrounds are treated as constants in time. The IBD detection efficiency is 80.25% with a correlated uncertainty of 1.19% [33] and an uncorrelated uncertainty of 0.13% among ADs. The oscillation parameters $\sin^2 2\theta_{13} = 0.0856 \pm 0.0029$ and $\Delta m_{ee}^2 = \left(2.522_{-0.070}^{+0.068}\right) \times 10^{-3}$ eV^2 from Ref. [6] are used to correct for the oscillation effect, namely $P_{ee}(E_\nu, L_{rd})$ in Eq. 1.

The time-averaged IBD yield, defined as the number of antineutrinos per fission times IBD cross section, is measured to be $(5.94 \pm 0.09) \times 10^{-43}$ cm^2/fission, where the statistical uncertainty is 0.05% and the systematic uncertainty is 1.5% taken from Table 1 in Ref. [33]. The corresponding average fission fractions for the four major isotopes ^{235}U, ^{239}Pu, ^{238}U and ^{241}Pu are 0.564, 0.304, 0.076, 0.056, respectively. The ratio of the measured IBD yield to the Huber-Mueller model prediction is 0.953 ± 0.014 (exp.) ± 0.023 (model).

The predicted prompt energy spectrum is determined from the $\bar{\nu}_e$ spectrum taking into account the effects of IBD kinematics, energy leakage and energy resolution. A model of the nonlinear energy response is used to correct the measured prompt energy spectrum of the IBD candidates [34] to facilitate comparison of spectra between different experiments [35]. The magnitude of the nonlinear

correction is $\sim 10\%$ at maximum with a 0.5% uncertainty at 3 MeV [34], improved from 1% previously [12]. Figure 1 shows the spectrum comparison of the measurement with the Huber-Mueller model prediction normalized to the measured number of events. The measurement and prediction show large discrepancy particularly near 5 MeV. With a sliding 2-MeV window scanning following Ref. [12], the largest local discrepancy is found in 4–6 MeV, with a significance of 6.3σ. The global discrepancy of the entire spectrum in 0.7–8 MeV has a significance of 5.3σ.
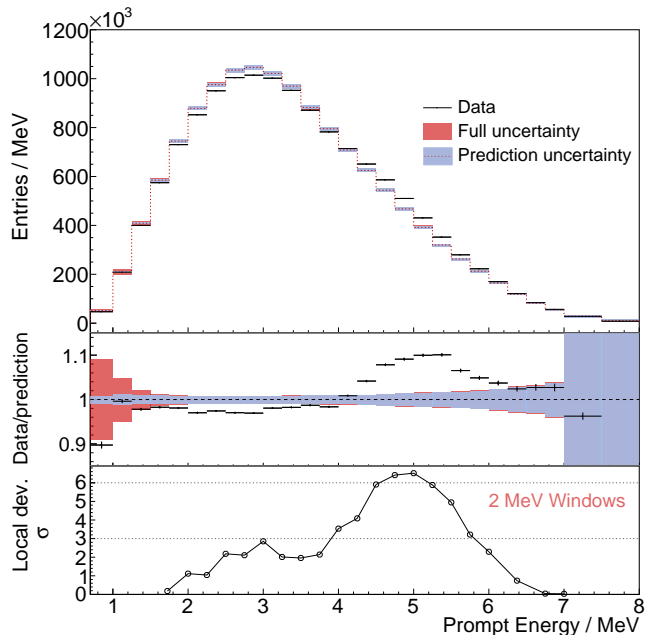

FIG. 1. (Top panel) Predicted and measured prompt energy spectra. The prediction is based on the Huber-Mueller model and is normalized to the number of measured events. The blue and red filled bands represent the square-root of diagonal elements of the covariance matrix for the flux prediction and the full systematic uncertainties, respectively. (Middle panel) Ratio of the measured prompt energy spectrum and the normalized predicted spectrum. The error bars on the data points represent the statistical uncertainty. (Bottom panel) The local significance of the shape deviation in a sliding 2-MeV window showing a maximum 6.3σ discrepancy in 4–6 MeV.

The evolution of fission fractions of the four major isotopes in multiple refueling cycles is shown in Fig. 2 for the six reactors during operation. The dominant isotopes contributing to the prompt spectrum are ^{235}U and ^{239}Pu, as their fission fractions add up to $\sim 87\%$. During a typical refueling cycle, ^{239}Pu is accumulated with fission fractions increasing from 15% to 38% while ^{235}U is consumed with fission fractions decreasing from 75% to 45%.

Each isotope produces a unique $\bar{\nu}_e$ spectrum depending on its fission products and corresponding beta-decay spectra [36, 37]. Since the observed prompt energy spectrum in one AD is a combination of the individual spectra of four isotopes, it evolves as a function of fission fractions [18, 22, 38]. In order
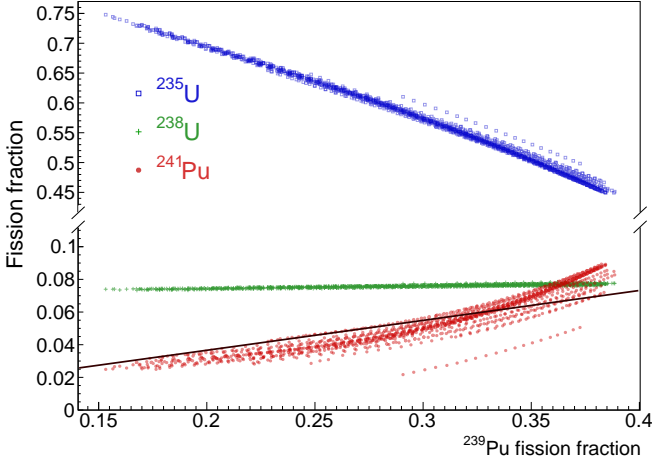
FIG. 2. The weekly fission fractions for the four major isotopes in the six reactors in 1958 days including four to six refueling cycles for each. The solid line represents an approximately linear relation between fission fractions of ^{239}Pu and ^{241}Pu.

to describe the relative contribution of each isotope in one AD from the six reactors, we define an effective fission fraction for isotope i observed by detector d as

$$f_{id}^{\text{eff}}(t) = \sum_r \frac{W_r(t)f_{ir}(t)}{L_{rd}^2 \sum_j f_{jr}(t)e_j} / \sum_r \frac{W_r(t)}{L_{rd}^2 \sum_j f_{jr}(t)e_j}. \quad (3)$$

The variation of detector-wise effective fission fraction of ^{235}U (^{239}Pu) is 50%–65% (24%–35%), smaller than the variation of reactor-wise fission fraction.

To explore the evolution of the IBD prompt energy spectrum, the data are divided into 20 groups ordered by the ^{239}Pu effective fission fraction in each week for each AD. The evolution of the prompt energy spectrum is dominated by ^{235}U and ^{239}Pu, while it is less sensitive to ^{238}U and ^{241}Pu due to smaller fission fractions. To extract the individual spectra of the ^{235}U and ^{239}Pu isotopes, $s^5(\eta^5)$ and $s^9(\eta^9)$ respectively, from the prompt energy spectrum, a χ^2 function in the Poisson-distributed form is constructed as

$$\chi^2(\eta^5,\eta^9) = 2\sum_{djk}(S_{djk}-M_{djk}+M_{djk}\ln\frac{M_{djk}}{S_{djk}})+f(\epsilon,\Sigma), \quad (4)$$

where d is the detector index, j is the index of the data groups, k is the prompt energy bin, M_{djk} is the measured prompt energy spectrum of each data group, ϵ is a set of nuisance parameters, $f(\epsilon,\Sigma)$ is the term to constrain the nuisance parameters incorporating systematic uncertainties and their correlations (Σ) among the reactors, detectors, and data groups, and

$$S_{djk} = \alpha_k(\epsilon)s_k^5(\eta_k^5)+\beta_k(\epsilon)s_k^9(\eta_k^9)+s_k^{238+241}(\epsilon)+c_k(\epsilon) \quad (5)$$

is the corresponding expected prompt energy spectrum without normalization, $s_k^5(\eta_k^5)$ ($s_k^9(\eta_k^9)$) is the element of extracted ^{235}U (^{239}Pu) spectrum at energy bin k, $\alpha_k(\epsilon)$

($\beta_k(\epsilon)$) is the corresponding coefficient for the ^{235}U (^{239}Pu) taking into account the detector target mass, detection efficiency, baseline and number of fissions, $s_k^{238+241}(\epsilon)$ is the expected prompt energy spectra contributed from ^{238}U and ^{241}Pu, and $c_k(\epsilon)$ includes contributions from the SNF, nonlinear nuclides, and backgrounds. The Huber-Mueller flux model is used to calculate the initial prompt energy spectrum for the four isotopes. Two sets of free parameters, η^5 and η^9, are applied to the 26 energy bins correcting the initial ^{235}U and ^{239}Pu spectra, respectively. As a result, the individual ^{235}U and ^{239}Pu spectra corrected with the best fit values of η^5 and η^9 do not depend on the input of the initial spectra. For the ^{238}U and ^{241}Pu spectra, nuisance parameters are incorporated to vary the initial spectra within their uncertainties. We conservatively enlarge the uncertainties of the ^{238}U and ^{241}Pu spectra quoted in the Huber-Mueller model based on the investigations of the antineutrino spectrum evaluations from nuclear databases [15, 17]. For the ^{238}U spectrum, the uncertainty is 15% in 0.7–4.5 MeV, 20% in 4.5–6 MeV, 30% in 6–7 MeV and 60% in 7–8 MeV, and for ^{241}Pu it is 10% in 0.7–7 MeV and 50% in 7–8 MeV. Additional normalization uncertainties of 15% and 10% [18] are assigned to the ^{238}U and ^{241}Pu spectra, respectively.

The time-dependence of reactor antineutrino production and detector response, and their impact on the ^{235}U and ^{239}Pu spectra, are examined. The drift of the energy scale is controlled to less than 0.1% using the calibration data and has negligible effect. The relative variation of energy resolution in the 20 data groups is 3% and has negligible effect on the extracted spectra. Therefore, the detector energy response [12] is treated as stable in the data-taking period, with its uncertainty treated as time-independent. The uncertainties of reactor power and fission fractions are treated as correlated between the data groups, and treating them as uncorrelated has a negligible effect in this analysis.

Performing the χ^2 fit with one energy bin covering the whole spectrum (0.7–8 MeV), we obtain the IBD yields of $(6.10\pm0.15)\times10^{-43}$ cm^2/fission and $(4.32\pm0.25)\times10^{-43}$ cm^2/fission for ^{235}U and ^{239}Pu, respectively. The statistical uncertainty contributes 10% (15%) of the total uncertainty and the systematic uncertainty contributes 90% (85%) for ^{235}U (^{239}Pu) IBD yield. The ratios to the expected IBD yield from the Huber-Mueller model are $0.920\pm0.023(\text{exp.})\pm0.021(\text{model})$ and $0.990\pm0.057(\text{exp.})\pm0.025(\text{model})$ for ^{235}U and ^{239}Pu, respectively, consistent with the previous analysis [18]. Removing the time-dependence of the nonequilibrium effect, SNF and nonlinear nuclides produces a shift of less than 0.7% in the IBD yields of ^{235}U and ^{239}Pu.

The top panel of Fig. 3 shows the extracted ^{235}U and ^{239}Pu spectra together with their Huber-Mueller predictions normalized to the best-fit numbers of events for ^{235}U (0.920) and ^{239}Pu (0.990), respectively. In the middle panel, the ratios of the extracted spectra to the corresponding predicted spectra for ^{235}U and ^{239}Pu are shown. An edge around 4 MeV is found in the ^{239}Pu spectrum compared to the prediction.

Analysis with different data grouping, or analysis with only EH1 or EH2 data shows a similar edge. In the energy window of 4–6 MeV, a 7% (9%) excess of events is observed for ^{235}U (^{239}Pu) spectrum compared with the normalized Huber-Mueller model prediction. A χ^2 test is performed to quantify the local discrepancy between the extracted ^{235}U and ^{239}Pu spectra and their corresponding predicted spectra following the method in Ref. [12]. As shown in the bottom panel of Fig. 3, the maximum local discrepancy is 4.0σ for the ^{235}U spectrum, and only 1.2σ for the ^{239}Pu spectrum because of larger uncertainties. If the ^{239}Pu spectrum is fixed to have the same spectral shape discrepancy as the ^{235}U spectrum in 4–6 MeV, we obtain a change in the χ^2 value, $\Delta\chi^2/$ndf = 4.0/8, corresponding to a 0.2σ inconsistency. Thus, the Daya Bay data indicates an incorrect prediction of the ^{235}U spectrum, but such a conclusion cannot be drawn for the other primary fission isotopes. Combining the results of IBD yield and spectral shape, we deduce that the 8% deficit of ^{235}U IBD yield is dominated by the deficit in the energy range below 4 MeV with a significance of 4σ with respect to the Huber-Mueller model prediction without normalization.
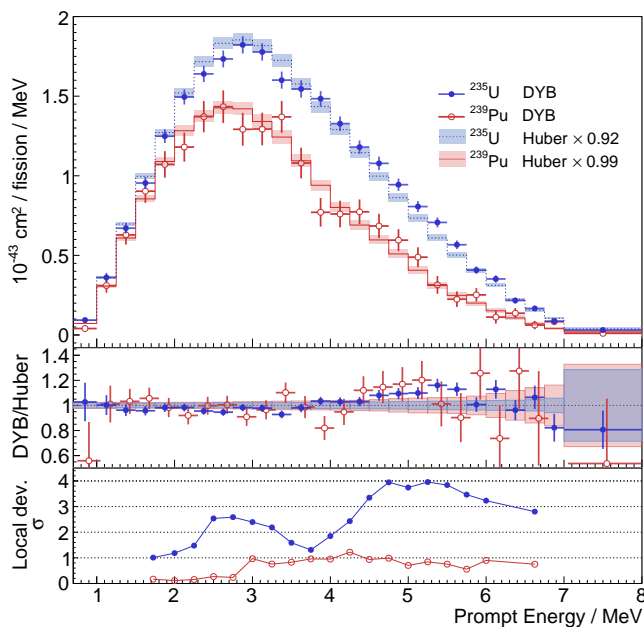

FIG. 3. (Top panel) Comparison of the extracted ^{235}U and ^{239}Pu spectra and the corresponding Huber-Mueller model predictions with the normalization factors 0.92 and 0.99, respectively. The error bars in the data points are the square root of the diagonal terms of the covariance matrix of the extracted spectra. The error bands are the uncertainties from the Huber-Mueller model. (Middle panel) Ratio of the extracted spectra to the predicted spectra. The ^{239}Pu data points are displaced for visual clarity of error bars. (Bottom panel) Local significance of the shape deviations for the extracted ^{235}U and ^{239}Pu spectra compared to the model predictions with a sliding 2-MeV window.

The fractional size of the diagonal elements of the covariance matrix is shown in the bottom panel of Fig. 4,

which is 4% for ^{235}U and 9% for ^{239}Pu around 3 MeV. The statistical uncertainty contributes to about 55% (60%) of the total uncertainty of ^{235}U (^{239}Pu). The uncertainties from the input ^{238}U and ^{241}Pu spectra and rate contribute about 35% for both ^{235}U and ^{239}Pu. The other uncertainties contribute to about 10% (5%) for ^{235}U (^{239}Pu). The spectral uncertainties of ^{235}U and ^{239}Pu are anti-correlated with correlation coefficients between -0.8 and -0.3. Any comparison of the ^{235}U or ^{239}Pu spectra with reactor flux models should take into account the correlations. The ^{235}U and ^{239}Pu spectra as well as their associated covariance matrix are provided in the Supplemental Material [39]. An independent analysis based on Bayesian inference using Markov Chain Monte Carlo with different data grouping obtains consistent results.

The extracted spectra of ^{235}U and ^{239}Pu have a certain dependence on the inputs of the ^{238}U and ^{241}Pu spectra. The ^{239}Pu spectrum has a larger uncertainty than ^{235}U because it has a smaller fission fraction and a strong correlation with ^{241}Pu. The fission fraction of ^{241}Pu is approximately proportional to ^{239}Pu as shown in Fig. 2, thus they can be treated as one component in the contribution to the prompt energy spectrum. A combination of ^{239}Pu and ^{241}Pu spectra (s_{239} and s_{241}), as an invariant spectrum independent of the fission fractions, is defined as $s_{\mathrm{combo}} = s_{239} + 0.183 \times s_{241}$. The coefficient of 0.183 is the average fission fraction ratio of ^{241}Pu to ^{239}Pu in 1958 days, shown as a line in Fig. 2. For 20 data groups, the fission fraction ratios of ^{241}Pu to ^{239}Pu evolve from 0.164 to 0.202 for the AD1 and AD2 in EH1, and from 0.171 to 0.191 for the AD3 and AD4 in EH2. The residual contribution of ^{241}Pu spectrum is corrected using Huber-Mueller model for some data groups when the fission fraction ratios of ^{241}Pu to ^{239}Pu deviate from 0.183. With this combination of ^{239}Pu and ^{241}Pu, the dependence on the input ^{241}Pu spectrum is largely removed. The top panel of Fig. 4 shows the extracted ^{235}U spectrum and s_{combo} compared with the normalized Huber-Mueller model predictions. The obtained ^{235}U spectrum and its uncertainty have negligible differences from the results shown in Fig. 3, since the systematic uncertainty of ^{235}U spectrum is dominated by the input ^{238}U spectrum instead of ^{241}Pu. The bottom panel shows the uncertainties of extracted spectra. The uncertainty of s_{combo} is 6% around 3 MeV, improved from 9% in the case of no combination. The maximal local significance of the spectral shape deviation is 1.4σ in the energy range of 4–6 MeV between the combined spectrum of ^{239}Pu and ^{241}Pu and the model prediction. The combined spectrum of ^{239}Pu and ^{241}Pu can be used to predict the $\bar{\nu}_e$ spectrum with higher precision in experiments with a similar fission fraction ratio of ^{241}Pu to ^{239}Pu.

In summary, an improved measurement of the prompt energy spectrum of reactor $\bar{\nu}_e$ is reported with a more precise energy response model and 1958 days of data from Daya Bay. The discrepancy between the measured spectrum shape and the prediction is found to be 5.3σ and 6.3σ in the entire energy range of 0.7–8 MeV and in a local energy range of
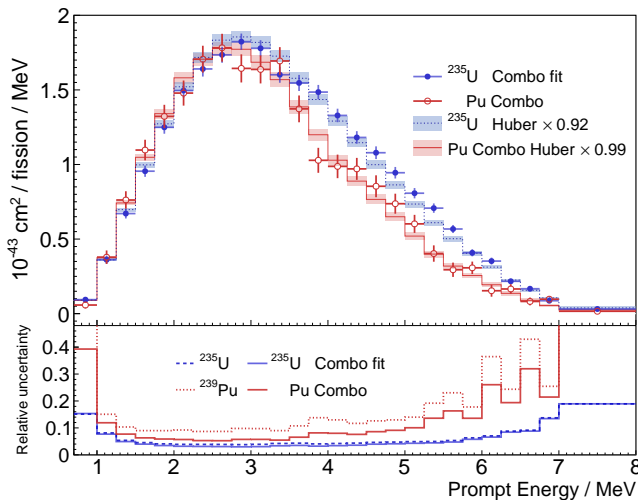
FIG. 4. (Top panel) Comparison of the extracted ^{235}U spectrum and s_{combo} as a combination of ^{239}Pu and ^{241}Pu with the corresponding Huber-Mueller predicted spectra with the normalization factors 0.92 and 0.99. (Bottom panel) The fractional size of the diagonal elements of the covariance matrix for extracted spectra with and without combination of ^{239}Pu and ^{241}Pu.

4–6 MeV, respectively. The IBD yields and prompt energy spectra of ^{235}U and ^{239}Pu as the two dominant components in commercial reactors are obtained using the evolution of the prompt spectrum as a function of fission fractions. A comparison of the measured and predicted ^{235}U and ^{239}Pu IBD yields prefers an incorrect prediction of the ^{235}U flux as the primary source of the reactor antineutrino rate anomaly. The spectral shape comparison shows similar excesses of events in 4–6 MeV for both ^{235}U (7%) and ^{239}Pu (9%). The discrepancy of 4.0σ in the comparison of spectrum shape for ^{235}U suggests incorrect spectral shape prediction for the ^{235}U spectrum. However, no such conclusion can be drawn for the ^{239}Pu spectrum due to a larger uncertainty.

* Now at Department of Chemistry and Chemical Technology, Bronx Community College, Bronx, New York 10453
[1] F. P. An et al. (Daya Bay Collaboration), Phys. Rev. Lett. 108, 171803 (2012).
[2] F. P. An et al. (Daya Bay Collaboration), Chin. Phys. C37, 011001 (2013).
[3] F. P. An et al. (Daya Bay Collaboration), Phys. Rev. Lett. 112, 061801 (2014).
[4] F. P. An et al. (Daya Bay Collaboration), Phys. Rev. Lett. 115, 111802 (2015).
[5] F. P. An et al. (Daya Bay Collaboration), Phys. Rev. D95, 072006 (2017).
[6] D. Adey et al. (Daya Bay Collaboration), Phys. Rev. Lett. 121, 241805 (2018).
[7] J. Ahn et al. (RENO Collaboration), Phys. Rev. Lett. 108, 191802 (2012).
[8] G. Bak et al. (RENO Collaboration), Phys. Rev. Lett. 121, 201801 (2018).
[9] Y. Abe et al. (Double Chooz Collaboration), Phys. Rev. Lett. 108, 131801 (2012).
[10] H. De Kerret et al. (Double Chooz Collaboration), (2019), arXiv:1901.09445 [hep-ex].
[11] F. P. An et al. (Daya Bay Collaboration), Phys. Rev. Lett. 116, 061801 (2016).
[12] F. P. An et al. (Daya Bay Collaboration), Chin. Phys. C41, 013002 (2017).
[13] S. H. Seo (RENO Collaboration), Proceedings, 26th International Conference on Neutrino Physics and Astrophysics (Neutrino 2014), AIP Conf. Proc. 1666, 080002 (2015).
[14] Y. Abe et al. (Double Chooz Collaboration), JHEP 10, 086 (2014).
[15] T. A. Mueller et al., Phys. Rev. C83, 054615 (2011).
[16] P. Huber, Phys. Rev. C84, 024617 (2011).
[17] G. Mention et al., Phys. Rev. D83, 073006 (2011).
[18] F. P. An et al. (Daya Bay Collaboration), Phys. Rev. Lett. 118, 251801 (2017).
[19] Y. J. Ko et al. (NEOS Collaboration), Phys. Rev. Lett. 118, 121802 (2017).
[20] V. Zacek, G. Zacek, P. Vogel, and J. L. Vuilleumier, (2018), arXiv:1807.01810 [hep-ex].
[21] Y. V. Klimov, V. I. Kopeikin, L. A. Mikalyan, K. V. Ozerov, and V. V. Sinev, At. Energ. 76, 123 (1994).
[22] G. Bak et al. (RENO Collaboration), (2018), arXiv:1806.00574 [hep-ex].
[23] M. Danilov (DANSS Collaboration), in 32nd Rencontres de Physique de La Valle d'Aoste (La Thuile 2018) La Thuile, Aosta, Italy, February 25-March 3, 2018 (2018) arXiv:1811.07354 [hep-ex].
[24] H. Kwon, F. Boehm, A. A. Hahn, H. E. Henrikson, J. L. Vuilleumier, J. F. Cavaignac, D. H. Koang, B. Vignon, F. Von Feilitzsch, and R. L. Mossbauer, Phys. Rev. D24, 1097 (1981).
[25] J. Ashenfelter et al. (PROSPECT Collaboration), (2018), arXiv:1812.10877 [nucl-ex].
[26] F. An et al. (JUNO Collaboration), J. Phys. G43, 030401 (2016).
[27] F. P. An et al. (Daya Bay Collaboration), Nucl. Instrum. Meth. A811, 133 (2016).
[28] P. Huber and P. Jaffke, Phys. Rev. Lett. 116, 122503 (2016).
[29] X. Ma et al., Phys. Rev. C88, 014605 (2013).
[30] K. Schreckenbach, G. Colvin, W. Gelletly, and F. Von Feil-

itzsch, Phys. Lett. **B160**, 325 (1985).

[31] F. Von Feilitzsch, A. A. Hahn, and K. Schreckenbach, Phys. Lett. **B118**, 162 (1982).

[32] A. A. Hahn *et al.*, Phys. Lett. **B218**, 365 (1989).

[33] D. Adey *et al.* (Daya Bay Collaboration), (2018), arXiv:1808.10836 [hep-ex].

[34] D. Adey *et al.* (Daya Bay Collaboration), (2019), arXiv:1902.08241 [physics.ins-det].

[35] In the previous spectrum measurements [11, 12], the energy response was not corrected in the measured prompt energy spectrum, but it was applied to the predicted energy spectrum.

[36] A. C. Hayes and P. Vogel, Ann. Rev. Nucl. Part. Sci. **66**, 219 (2016).

[37] A. A. Sonzogni, E. A. McCutchan, and A. C. Hayes, Phys. Rev. Lett. **119**, 112501 (2017).

[38] P. Huber, Phys. Rev. Lett. **118**, 042502 (2017).

[39] See Supplemental Material at [URL will be inserted by publisher] for the following tabulated data: the effective fission fractions of four isotopes in 20 data groups for 4 ADs, the ^{235}U and ^{239}Pu spectra and their covariance matrix, the ^{235}U and the combined ^{239}Pu and ^{241}Pu spectra and their covariance matrix, the correction of SNF, nonequilibrium, and nonlinear nuclides in 20 data groups for 4 ADs, the ^{235}U and ^{239}Pu spectra and their covariance matrix in the case of without any correction of SNF, nonequilibrium and nonlinear nuclides.